separations

MDPI

Article

Removal of Pb(II) from Aqueous Solution and Adsorption Kinetics of Corn Stalk Biochar

Wenling Yang [1], Chaoyang Lu [2], Bo Liang [3], Chaohui Yin [2], Gao Lei [1], Baitao Wang [1], Xiaokai Zhou [2], Jing Zhen [1], Shujing Quan [1] and Yanyan Jing [2,*]

[1] Institute of Biology Co., Ltd., Henan Academy of Sciences, Zhengzhou 450008, China
[2] Key Laboratory of New Materials and Facilities for Rural Renewable Energy (Ministry of Agriculture and Rural Affaires of China), Henan Agricultural University, Zhengzhou 450002, China
[3] Henan High Tech Industrial Co., Ltd., Henan Academy of Sciences, Zhengzhou 450008, China
* Correspondence: jingyanyan123@126.com

Abstract: In this work, the Pb adsorption and removal ability of biochar from simulated Pb(II)-contaminated wastewater, adsorption isotherms, kinetics, and thermodynamics were studied. Adsorption characteristics of biochar on Pb(II) were analyzed by Fourier transform infrared spectroscopy (FT-IR), X-ray diffraction (XRD) and scanning electron microscope with energy dispersive spectrometer (SEM-EDS). The influence of the pH of the solution, the contact time, and the biochar dose on the removal of Pb(II) were investigated by single-factor design and response surface analysis. With the increase in biochar dose from 2 g/L to 4 g/L in wastewater, the Pb(II) amount adsorbed on biochar reduced from 21.3 mg/g to 17.5 mg/g. A weakly acidic environment was more conducive to the ligand exchange between Pb(II) ions and biochar. Pb(II) adsorption kinetics of biochar showed that the Pseudo-first-order model was more suitable than other employed models to describe the adsorption process. During the isothermal adsorption process, Langmuir and Freundlich's isotherms fitted the adsorption data very well (R^2 > 96%). The Pb (II) adsorption onto biochar was spontaneous in the specified temperature range (298–318 K) and the process was exothermic. Simultaneously, the optimal conditions were a pH of 5, a contact time of 255 min, and a biochar dose of 3 g/L, under which the maximum predicted Pb(II) removal efficiency was 91.52%.

Keywords: biochar; Pb(II) removal; adsorption ability; kinetic analysis

Citation: Yang, W.; Lu, C.; Liang, B.; Yin, C.; Lei, G.; Wang, B.; Zhou, X.; Zhen, J.; Quan, S.; Jing, Y. Removal of Pb(II) from Aqueous Solution and Adsorption Kinetics of Corn Stalk Biochar. *Separations* **2023**, *10*, 438. https://doi.org/10.3390/separations10080438

Academic Editors: Yingjie Li and Senlin Tian

Received: 15 June 2023
Revised: 20 July 2023
Accepted: 25 July 2023
Published: 2 August 2023

1. Introduction

With the increase in economic development and social demand, the amount of Pb-containing wastewater discharged from numerous sources increases sharply [1]. Pb is not only highly toxic but also difficult to degrade [2]. After discharge, the Pb-contaminated wastewater will be utilized and absorbed by plants causing the accumulation of a large amount of Pb in the plant body. Excessive Pb intake may result in the destruction of the plant cell structure and eventually in plant damage or death [3]. Pb can also be absorbed through water, air, food, and skin, entering various body organs and causing diseases such as anemia, kidney damage, and nervous system disorders through accumulation in the body [4,5]. Therefore, effective treatment of Pb-contaminated wastewater before discharge is of great significance to control heavy metal pollution and protect human health.

The main treatment methods for Pb-contaminated wastewater include chemical precipitation, ion exchange, membrane filtration, and adsorption [6,7]. Among them, the adsorption method is considered to be a suitable method for removing pollutants in wastewater due to its convenient operation and high removal efficiency. However, the excessively high cost of adsorbent makes it limited in the treatment of wastewater containing heavy metals. Therefore, searching for adsorption materials with a wide range of materials, high efficiency, low cost, and high environmental stability has gradually become a research hotspot in the field of adsorption.

In recent years, biomass raw materials represented by straw, spent mushroom substrate, livestock manure, and industrial sludge have attracted widespread attention. Most of these biomass raw materials are derived from by-products or wastes in industrial and agricultural production processes. They have great application prospects in the field of adsorption with a wide range of sources and low cost [8–11]. However, the direct use of biomass raw materials as adsorbents is inefficient. A previous report revealed that the untreated corn straw particles showed the maximum adsorption capacity (15.0269 mg/g) for Pb(II) [12].

Biochar is an alkaline carbon-based material that contains a certain amount of oxygen and hydrogen in the form of functional groups on its surface [13]. Moreover, biochar consists of a multi-pore structure with a large specific surface area [14,15], which can fully contact with gas, liquid, and other media, whereby the functional groups on the pore walls of biochar exhibit a high affinity for impurities which can be absorbed into the pores [2]. China is a largely agricultural country with abundant straw resources, especially in Henan province, but the utilization rate of straw is low, less than 40%. The processing of straw to biochar for the removal of heavy metals in wastewater not only realizing the resource utilization of straw waste, but also recover Pb by burning Pb-loaded biochar (compared with incombustible sorbents), which supports the long-term strategy of carbon emission reduction.

Biochar is widely used to treat Pb pollution in water because of its porosity and stability [16], and the maximum adsorption capacity of wheat straw biochar for Pb(II) reached 149.7 mg/g [17]. Xue et al. [18] examined the effect of H_2O_2 treatment on hydrothermally produced biochar (hydrochar) from peanut hull to remove aqueous heavy metals and found that the modified hydrochar-enhanced Pb(II) sorption ability with a sorption capacity of 22.82 mg/g, which was comparable to that of commercial activated carbon and was more than 20 times of that of untreated hydrochar (0.88 mg/g). While the maximum Pb(II) adsorption capacity (Q_m) of biochar from peanut shells was 56.5 mg/g at the optimum conditions. The adsorption followed pseudo-second-order kinetics, and the equilibrium data were well-fitted with the Langmuir isotherm. The adsorption process was feasible and spontaneous at all temperature values that were tested, and the process was exothermic [19]. Wang et al. [20] compared the adsorption effects of cotton straw-derived biochar under different pyrolysis conditions on Pb (II) and found the pyrolysis temperature had a significant effect. The maximum adsorption capacity of 124.7 mg/g was obtained at 600 °C with an optimal pH of 5.5. The isothermal adsorption curve of Pb (II) was in line with the Langmuir model, while the Pb (II) adsorption kinetics followed the pseudo-second-order model indicating that chemical adsorption or physical chemistry adsorption dominated the adsorption mechanism. However, Liu et al. [21] reported that corn stalk biochars generated at a pyrolytic temperature of 450 °C was an ideal sorbent with the maximum Pb(II) adsorption capacity, in which the maximum Pb(II) adsorption capacity (Q_m) of CSB450 was 49.70 mg/g at the optimal condition. These results presented variable Pb (II) sorption efficiency of the tested biochars. This variability may be caused by many factors, such as the source and composition of the original waste material, pyrolysis temperature, different sorption mechanisms, as well as the adsorption conditions [9,16,20,22,23]. Therefore, it is necessary to carry out special works for each heavy metal ion and adsorbent pair to identify superior adsorbents. In recent years, although research on this subject is ongoing, to date, researchers have not yet been able to determine the most suitable adsorbent to remove Pb(II) ions from wastewater. Therefore, it is necessary to explore the sorption mechanisms of heavy metals on biochar to improve the heavy metal removal efficiency and guide the future application of local corn straw biochar. Therefore, in the present study, the Pb(II) removal ability of corn stalk biochar and the kinetic properties were studied, response surface methodology (RSM) was used to optimize the Pb(II) adsorption process, and then the sorption mechanisms of Pb(II) on biochar were explored.

2. Materials and Methods

2.1. Preparation of Biochar

Corn stalks collected in Zhengzhou, Henan province, China. The naturally dried corn stalk samples were crushed, ground through 80 mesh sieve and placed in a muffle furnace at a heating rate of 10 °C/min to 500 °C and kept for 2 h to obtain corn stalk biochar.

2.2. Characterization of Biochar

Element composition of corn stalk biochar (80 mesh) was determined by a Vario EL Cube elemental analyzer (Elementar Analysensysteme GmbH, Hanau, Germany). The carrier gas (O_2) pressure was 0.20 MPa, and the protective gas (He) pressure was 0.12 MPa.

Using N_2 and He as carrier gases at 103 kPa, the specific surface area of biochar was determined by a BELSORP-mini II instrument (BEL, Osaka, Japan). The specific surface area test specification was greater than 0.01 m^2/g.

The surface morphology of biochar was examined using the scanning electron microscope (SEM, JSM-6510, Tokyo, Japan) equipped with the energy-dispersive X-ray spectroscope (EDS, EX-94400T4L11, Tokyo, Japan). The X-ray diffraction (XRD) of biochar samples was characterized using Smart Lab 3 kW diffractometer (Rigaku Corporation, Tokyo, Japan) equipped with Cu Kα radiation.

A Fourier transform infrared (FT-IR) spectrometer (Ruian Technology Co., Ltd., Tianjin, China) was used for the qualitative and quantitative analysis of biochar samples [24]. Potassium bromide (KBr) was used as the scanning background spectrum. The scanning range was 4000–400 cm^{-1}, and the resolution was 0.5 cm^{-1}.

To quantify the pH at the zero point of charge (pH_{ZPC}), 0.1 g of carbon was added to 20 mL of 0.1 M NaCl solution, and the initial pH value of the solution was adjusted by adding HCl or NaOH from 2 to 11 (pH = 2, 3, 4, 5, 6, 7, 8, 9, 10, 11). The containers were placed in a thermostatic shaker maintained at 25 ± 2 °C and operated at a rotation speed of 150 rpm for 24 h, after which the pH was measured. pH_{ZPC} is the pH measured when there is no change in pH after contact with carbon [25,26].

2.3. Adsorption Ability of Biochar

The adsorption experiments were conducted in triangle bottles. Working solutions of Pb(II) prepared using $Pb(CH_3COO)_2{\cdot}3H_2O$ and biochar were added to each triangle bottle, which was sealed and placed in a thermostatic shaker maintained at 25 ± 2 °C and operated at a rotation speed of 150 rpm. The main parameters that affect biochar adsorption were varied, including the dose of biochar (0.5, 1, 2, 4, 6 g/L), pH (2, 3, 4, 5, 6, 7), contact time (10 to 1 440 min), and the concentration of Pb(II) (100, 200, 300, 500, 700, 1000 mg/L). The pH value was adjusted by adding HCl or NaOH and measured with a digital pH meter (China FE28). The chemicals and reagents were all purchased from Zhengzhou paini company (Zhengzhou, China).

After Pb(II) adsorption experiments, the biochar was separated from the Pb(II)-contaminated aqueous solution by a 0.45-micron filter membrane, and 5 mL of the filtrate were subsequently sampled with a syringe for analysis. The initial and residual concentrations of Pb(II) in the aqueous solutions were determined by an AA-6880F/AAC atomic absorption spectrophotometer (Shimadzu, Tokyo, Japan) with a wavelength of 283.3 nm and a wavelength accuracy of ±0.3 nm. The instrument was operated under the output pressure of 0.35 MPa of an air compressor and the outlet pressure of 0.09 MPa. The pressure of the carrier gas (C_2H_2) was greater than 0.5 MPa. The removal efficiency (%) of Pb from the contaminated water was determined by Equation (1) and the adsorption amount (mg/g) as shown in Equation (2) [27]. Each step of the experiment was conducted in triplicate.

$$R = \frac{C_0 - C_t}{C_0} \times 100, \tag{1}$$

$$Q = \frac{(C_0 - C_t)V}{m}, \tag{2}$$

where C_0 and C_t are the measured Pb(II) concentrations (mg/L) by atomic absorption spectrophotometer before adsorption and after a specific time of adsorption (t, min), V is the volume of the Pb(II)-contained aqueous solution, and m is the mass of biochar (g).

2.4. Adsorption Kinetics of Biochar

Adsorption kinetics refers to the adsorption process as a function of adsorption amount over adsorption time. A volume of 25 mL of the prepared 100 mg/L Pb(II) working solution and 0.1 g biochar were added into a 100 mL triangle bottle to prepare an adsorption solution with a biochar dose of 4 g/L. The triangle bottles were placed in a constant temperature shaker and shaken for 10–1440 min. The Pb(II) adsorption kinetics of biochar were analyzed using a Pseudo-first-order model, Pseudo-second-order model, and the Elovich model.

$$\text{Pseudo-first-order}: \ Q_t = Q_e\left(1 - e^{-k_1 t}\right), \tag{3}$$

$$\text{Pseudo-second-order}: \ Q_t = \frac{Q_e^2 k_2 t}{1 + Q_e k_2 t}, \tag{4}$$

$$\text{Elovich}: \ Q_t = \frac{1}{\beta}\ln(\alpha\beta t + 1), \tag{5}$$

where Q_t and Q_e are the adsorption amount (mg/g) at t time and at adsorption equilibrium, respectively [28]; k_1 is Pseudo-first-order kinetic model constant (min^{-1}) [29]; k_2 is Pseudo-second-order kinetic model constant (g/(mg·min)) [30]; α is the adsorption rate (mg/(g·min)) at zero point; β is a constant (g/mg) related to surface coverage and chemisorption activation energy [31].

2.5. Adsorption Isotherms

Isothermal adsorption was carried out at a biochar dose of 4 g/L, a pH of 5, a contact time of 240 min, and in the Pb(II) solution concentration range of 100–1000 mg/L (100, 200, 300, 500, 700, and 1000 mg/L). Langmuir model and Freundlich model were used to fit the adsorption data.

$$\text{Langmuir}: \ Q_e = \frac{kQ_m C_e}{1 + kC_e}, \tag{6}$$

$$\text{Freundlich}: \ Q_e = k_f C_e^n, \tag{7}$$

where Q_e is the adsorption amount (mg/g) at adsorption equilibrium; Q_m is the theoretical maximum adsorption amount (mg/g); k is the Langmuir isothermal equation constant (L/mg); n is the empirical constant related to adsorption strength; k_f is Freundlich isothermal equation constants; C_e is the Pb(II) concentration (mg/L) at adsorption equilibrium [32].

2.6. Thermodynamic Analysis

In order to explored interaction occurring at the interface biochar/Pb(II), thermodynamic analysis of Pb(II) adsorption onto corn stalk biochar was detected by the adsorption performing at variable temperatures (298 K, 308 K, and 318 K).

$$\ln K_q = \frac{\Delta S^0}{R} - \frac{\Delta H^0}{RT}, \tag{8}$$

$$\Delta G^0 = \Delta H^0 - \Delta S^0 \cdot T. \tag{9}$$

The parameters of adsorption thermodynamic as entropy (ΔS^0, J/mol·K), enthalpy (ΔH^0, kJ/mol), and the Gibbs free energy (ΔG^0, kJ/mol) were measured referring to Equations (8) and (9), where T is absolute temperature K; K_q (L/g) is the distribution coefficient of adsorbent that equals to Q_e/C_e, and R = 8.314 J/mol·K.

3. Results and Discussion

3.1. The Properties of Biochar

The element composition and specific surface area of corn stalk biochar were shown in Table 1. Corn stalk biochar was mainly composed of C, H, N, and S, in which the highest percentage of C mass was 49.15%, and the lowest percentage of S mass was 0.16%. The total volume of biochar was 1.71×10^{-2} cm^3/g, with an average pore diameter of 20.32 nm and the specific surface area was 3.36 m^2/g.

Table 1. Main element composition and specific surface area of biochar.

C (%)	H (%)	N (%)	S (%)	C/H	C/N	Total Volume (cm^3/g)	Pore Diameter (nm)	Specific Surface Area (m^2/g)
49.15	1.81	0.95	0.16	27.20	52.16	1.71×10^{-2}	20.32	3.36

The SEM-EDS images of the biochar before and after Pb(II) adsorption were shown in Figure 1. Without Pb(II) present (Figure 1a), the material had a fluffy, porous texture with a large, accessible surface area that favored sorption (physical sorption). The Pb(II) loaded biochar (Figure 1b) showed a surface that is less fluffy. The EDS spectra (Figure 1c,d) showed that Pb(II) adsorption occurred at the surface of the biochar and presumably in the pores in the material, indicating uptake of Pb(II).

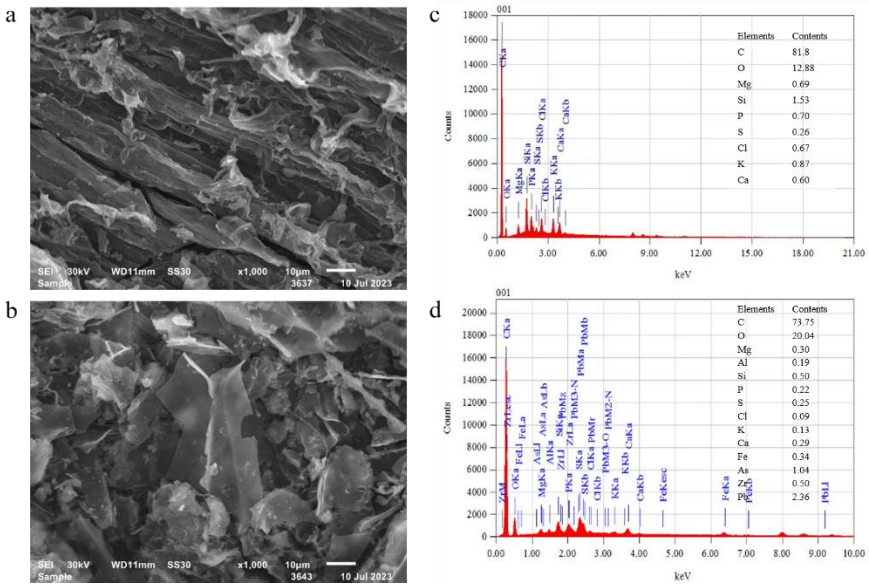

Figure 1. SEM and EDS spectra image analysis of biochar before (**a**,**c**) and after (**b**,**d**) Pb(II) adsorption.

To compare the changes of functional groups presented on the biochar surface, FT-IR spectroscopy was used to analyze the biochar before and after Pb(II) adsorption at a biochar dose of 4 g/L. The spectra were shown in Figure 2. After the adsorption of Pb(II), some functional groups on the biochar surface combined with Pb(II) ions. The peaks at 1048, 1408, 1633, and 3466 cm^{-1} represented the C-O, C-H, C=O, O-H, and stretches, respectively. Although the FT-IR peak position of biochar before and after Pb(II) adsorption has not changed greatly, the absorbed energy has changed, resulting in great changes in infrared transmittance before and after Pb(II) adsorption on biochar. O-H stretching (3466 cm^{-1}) decreased after the adsorption of Pb(II), suggesting the breakage of O-H bonds after Pb(II) adsorption. Some oxygen-containing functional groups, such as C=O, O-H and C-O, existed on the surface of the biochar, which provided a negative charge (COO-/OH-) adsorbing Pb(II) on its surface [33]. By comparing the two FTIR patterns, it can be seen that there was a significant decrease in the number of peaks that appeared, which was due to the reaction of these functional groups with the Pb(II) ions during the adsorption process.

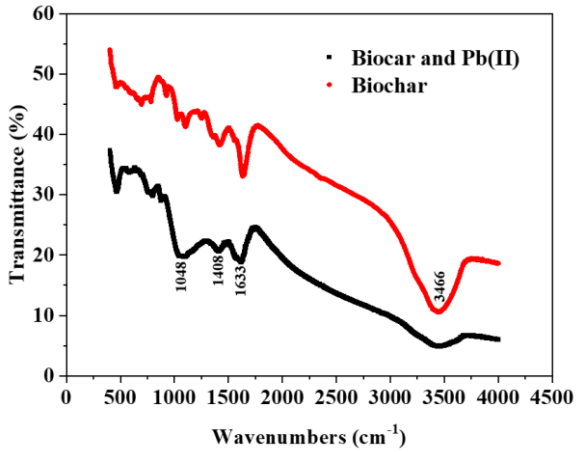

Figure 2. FT-IR of biochar before and after Pb(II) adsorption.

To characterize the crystallinity of samples, the XRD pattern of biochar before and after Pb(II) adsorption was shown in Figure 3. In the diffraction area of 15°–35°, obvious diffraction peaks can be observed on the biochar after Pb(II) adsorption. By comparing the peak changes before and after adsorption, it was found that the peak strength after adsorption of Pb(II) was enhanced at 24.50°, 29.93°, and 33.95° compared with biochar without Pb(II), indicating the presence of hydroxypyromorphite ($Pb_5(PO_4)_3OH$) and hydrocerussite ($Pb_3(CO_3)_2(OH)_2$) [34].

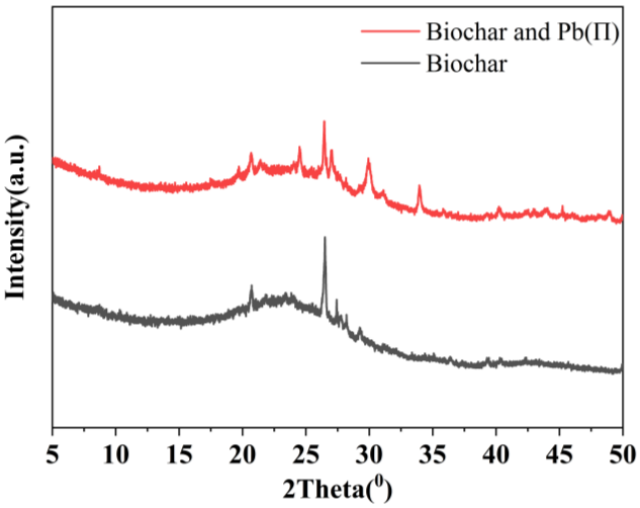

Figure 3. XRD pattern of biochar before and after Pb(II) adsorption.

It is well known that pH_{zpc}, which is indicative of the types of active centers on the surface and the adsorption mobility of the surface, is an important factor in adsorption processes. The pH_{zpc} value was obtained from the correlation of the differences between the initial and final measured pH, which was performed on ΔpH. Then, ΔpH was plotted versus the initial pH, as observed in Figure 4. The observed point where the edge surface exhibits no charge is pH_{zpc} = 7.65 for the biochar. According to the literature, such results may infer that when pH solution < 7.65 (pH_{zpc}), the biochar surface tends to exhibit a positive charge and when pH solution > 7.65 (pH_{zpc}) the biochar surface tends to present a negative charge. But, it is well known that at pH levels greater than 6 in Pb(II) solutions, $Pb(OH)_2$ is formed and precipitates in the aqueous media. For these reasons, the pH range of 5–6 was considered to be more suitable for the removal of Pb(II) ions.

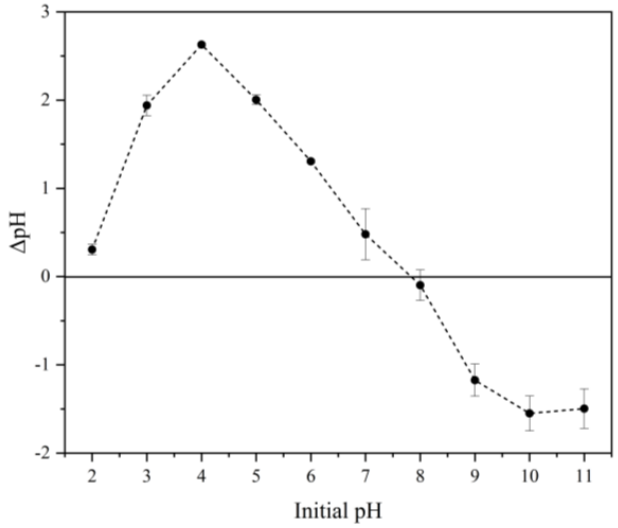

Figure 4. pH variation between final and initial pH measurements of the biochar.

3.2. Effect of Biochar Dose on Pb(II) Removal

The influence of biochar dose on the adsorption effect for Pb(II) is shown in Figure 5. This experiment was conducted at an initial Pb(II) concentration of 100 mg/L and an adsorption contact time of 1 440 min. With the increase in biochar dose from 0.5 g/L to 2 g/L in wastewater, the Pb(II) amount adsorbed on biochar increased rapidly from 2.6 mg/g to 21.3 mg/g, and the Pb(II) removal efficiency increased to 42.66%. When the biochar dose was increased to 4 g/L and 6 g/L, the residual Pb(II) concentration decreased rapidly (from initial 100 mg/L to 26.0 mg/L and 17.9 mg/L), and the Pb(II) removal efficiency increased to 73.99% and 82.13%, respectively. However, the adsorption amounts of Pb(II) decreased gradually to 17.5 mg/g and 13.6 mg/g for the biochar doses of 4 g/L and 6 g/L. It is evident that a high dose of adsorbent is required for the quantitative removal of heavy metal, but the removal efficiency of pollutants should be considered comprehensively at the same time. As an explanation for this observation, the number of active sites for Pb(II) adsorption increased with the increase in the adsorbent amount [35], but the content of Pb(II) in the solution was limited resulting in an excess of adsorption sites [36]. As a consequence, although the removal efficiency of biochar increased, the adsorption amount per unit mass of biochar decreased.

3.3. Effect of pH on Pb(II) Removal

Using an initial Pb(II) concentration of 100 mg/L, an adsorption contact time of 1440 min, and a biochar dose of 4 g/L, the influence of the solution pH value (pH = 2, 3, 4, 5, 6, 7) on the Pb(II) adsorption by biochar was investigated. The results were shown in Figure 6. Considering the competitive adsorption of H^+ and Pb(II) [37] and that the content of H^+ in solution decreased with increasing pH from 2 to 5, the degree of protonation of functional groups on the surface of biochar decreased, which was conducive to the adsorption of positively charged Pb(II). The removal efficiency of Pb(II) reached a maximum of 83.35% at pH 5. The Pb(II) adsorption capacity of biochar was greater than 19.0 mg/g at pH 5–7. However, $Pb(OH)_2$ is formed in the aqueous media under pH > 6. Therefore, when the solution pH was greater than 6, the Pb(II) removal not only included the adsorption by biochar but also included some $Pb(OH)_2$ precipitation. Compared to pH 5, the Pb(II) removal efficiency of biochar at pH 6 and 7 decreased slightly (82.86% and 80.25%, respectively). According to these findings, the weak acidic condition was beneficial for the ligand exchange between heavy metal ions and biochar, demonstrating a better removal effect.

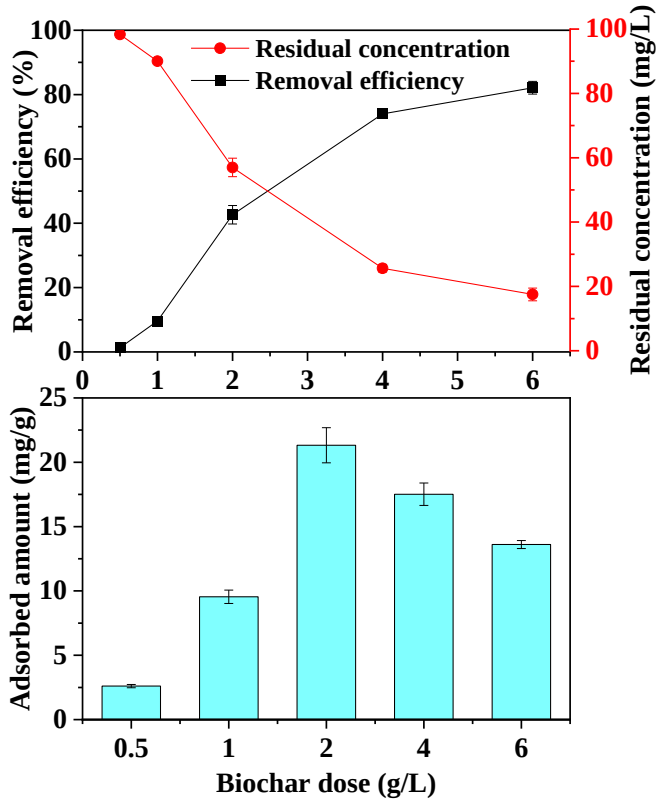

Figure 5. Effect of biochar dose on the Pb(II) removal.

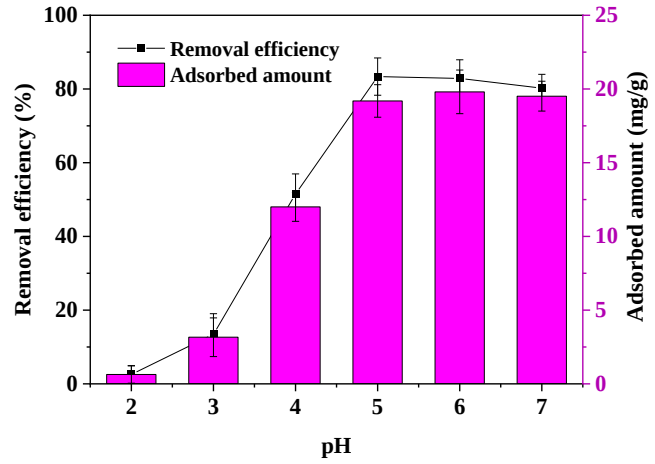

Figure 6. Effect of pH on the Pb(II) adsorption.

3.4. Pb(II) Adsorption Kinetics of Biochar

Figure 7 showed the Pb(II) adsorption kinetics of biochar at a range of contact times from 10 min to 1 440 min, an initial Pb(II) concentration of 100 mg/L, a pH of 5, and a biochar dose of 4 g/L. In the early stages of adsorption, the adsorption amount of Pb(II) increased rapidly within 90 min and reached 18.6 mg/g. In the period of 90–240 min, the adsorption amount of Pb(II) continued to increase, reaching 20.8 mg/g at 240 min, but the rate of increase was slow. Since, the mass transfer driving force caused by the concentration difference of Pb(II) in the water–biochar phase system enhanced the capacity of directional migration of adsorbates [38], which allowed the adsorption molecules to enter the internal pores in parallel. After a certain contact and adsorption time, the number of adsorption sites on the surface of biochar decreased, the diffusion path of Pb(II) in the

biochar was prolonged [39], and the increase in the adsorption amount over the same period declined significantly.

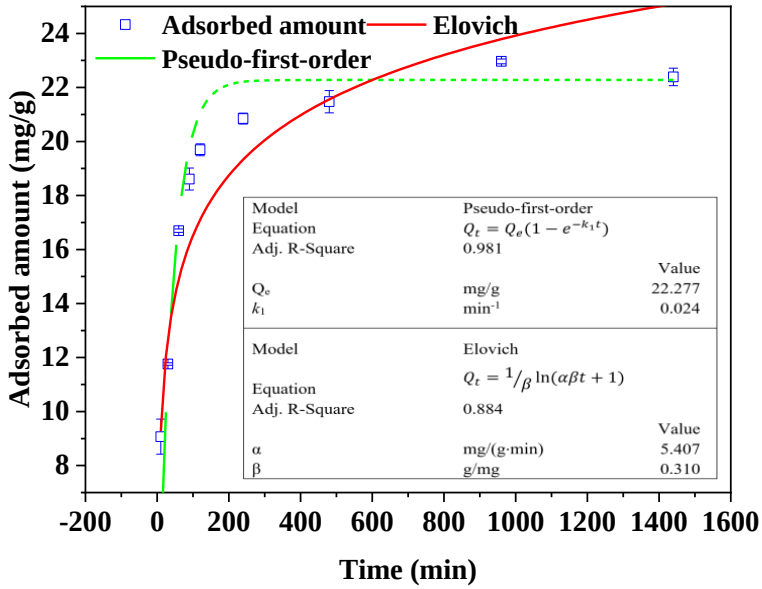

Figure 7. Pb(II) adsorption kinetics of biochar.

The Pseudo-first-order model, Pseudo-second-order model and Elovich model were used to analyze the Pb(II) adsorption kinetics of biochar. It was found that Pseudo-first-order model was suitable to describe Pb(II) adsorption, with a correlation coefficient (R^2) of 98.1%. The adsorption amount of Pb(II) at adsorption equilibrium was 22.277 mg/g, which was only about 1.5 mg/g higher than the adsorbed amount at 240 min (20.8 mg/g). The Elovich model simulated the Pb(II) removal effect of biochar, and the R^2 was 88.4%. In the early stage of adsorption, the concentration of Pb(II) was high and the mass transfer driving force of the solution was large, resulting in Pb(II) easily overcoming the mass transfer resistance between liquid and solid interfaces [23]. In addition, due to the large number of unsaturated adsorption sites on the surface of biochar, Pb(II) was easier adsorbed, and the adsorption amount increased rapidly. The adsorption rate at the zero point was 5.407 mg/(g·min). With increasing contact time between Pb(II) and biochar, the Pb(II) concentration in the wastewater gradually decreased, leading to the decrease in the Pb(II) concentration difference at the solid–liquid interface; the adsorption sites on the surface of biochar became saturated, and the adsorption rate decreased. The constant value of the activation energy of the β reaction in the model was 0.310, indicating that the low activation energy of biochar for the adsorption of Pb(II) resulted in a fast adsorption rate. However, the Pseudo-second-order model was not suitable to describe the observed Pb(II) adsorption kinetics of biochar.

3.5. Isothermal Adsorption of Pb(II) Removal

As shown in Figure 8, the removal efficiency of Pb(II) decreased rapidly at initial Pb(II) concentrations of 100, 200, and 300 mg/L. At an initial Pb(II) concentration of 100 mg/L, the maximum removal efficiency was 90.31%, and the adsorption amount was 21.6 mg/g. At higher Pb(II) concentrations, the removal efficiency continued to decrease and finally tended to be stable. With a further increase to 500 mg/L, the adsorption amount was 37.1 mg/g, and the removal efficiency was reduced to 32.08%. Based on these results, corn stalk biochar exhibited a good ability to adsorb Pb(II) and could be used as adsorption material for low concentrations of Pb(II) in solution.

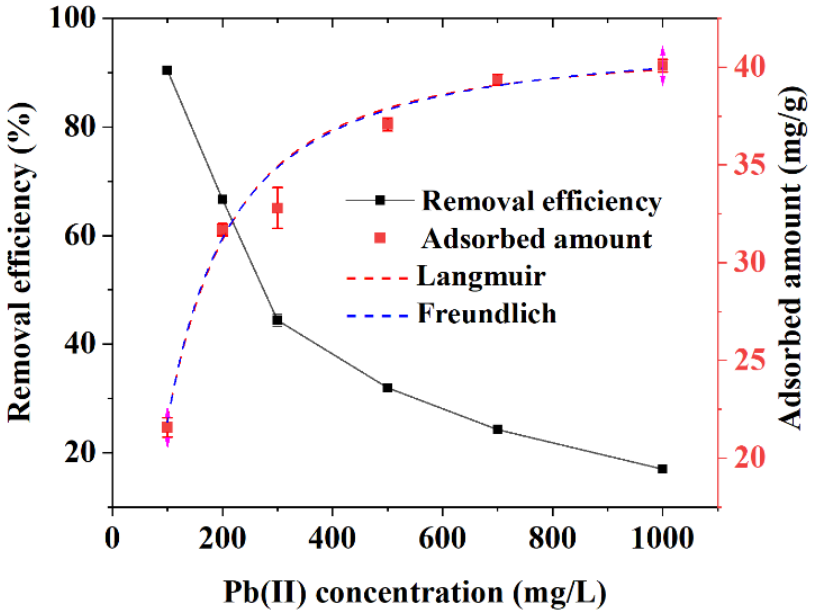

Figure 8. Isotherm adsorption of biochar on Pb(II) removal.

To further clarify the Pb(II) adsorption mechanism on biochar, Langmuir and Freundlich isothermal models were used to fit the adsorption data of Pb(II). Correlation coefficients of 99.8% fitting by the Langmuir model were shown in Table 2, which indicated it was suitable to describe Pb(II) adsorption. And, the maximum adsorption amount predicted by Langmuir model was 40.984 mg/g, which was similar with actual Pb(II) adsorption by biochar under concentrations of 1000 mg/L. The application of the Freundlich model resulted in a good fit (R^2 = 96.5%), which indicated that the surface of biochar was heterogeneous, and the adsorption of Pb(II) on biochar was dominated by heterogeneous adsorption with multi-molecular layers. These were different from magnetized activated carbon prepared by hydrothermal method using rape straw powder. The adsorption of magnetized activated carbon was mainly determined by surface electrostatic attraction, surface complexation and co-precipitation, and magnetized activated carbon had a large adsorption capacity for Pb(II) (253.2 mg/g) and Cd(II) (73.3 mg/g) [40]. The empirical constant *n* of the Freundlich model was 0.138 (Table 2) in the range of 0–1, indicating that biochar was favorable for the adsorption of Pb(II), and the process proceeded easily [41]. The adsorption resistance was small, and the adsorption force was large at low Pb(II) concentrations in the solution (removal efficiency: 90.31% at 100 mg/L) (Figure 8). However, the number of adsorbed molecular superposition layers increased continuously, and the adsorption force decreased continuously with the increase in the adsorption amount for solutions of high Pb(II) concentrations. Thus, the removal efficiency was only 17.15% (Figure 8) at an initial Pb(II) concentration of 1000 mg/L.

Table 2. Correlation coefficients for the isotherm adsorption.

Langmuir			Freundlich		
Q_m (mg/g)	k (L/mg)	R^2	k_f	n	R^2
40.984	0.041	0.998	16.443	0.138	0.965

3.6. Thermodynamic Analysis of the Adsorption Process

To determine the endothermic or exothermic behavior of biochar adsorption on Pb(II), the study of the temperature influence on the adsorption process by biochar was investigated. In addition, the obtained values of thermodynamic parameters (Gibbs free energy (ΔG^0), enthalpy (ΔH^0), and entropy (ΔS^0)) were listed in Table 3. The values of Gibbs free

energy change (ΔG^0) were negative values, that was, the Pb (II) adsorption onto biochar was spontaneous in the specified temperature range (298–318 K). Also, the increase in the values of ΔG^0 as the temperature increased indicated that high temperature hindered the adsorption, and 25 °C (298 K) was more conducive to the adsorption process. Moreover, ΔH^0 presented with a negative value (−9.152 kJ/mol) indicating that the adsorption was an exothermic process, further proving that low temperature was conducive to the adsorption in the range of 298–318 K. The negative value of entropy (ΔS^0 = −20.576 (J/mol·K) confirmed that the adsorption by biochar on Pb(II) was a process of entropy reduction, and the randomness of the interface between biochar and Pb(II) was small. The adsorption process of methylene blue on corn cob-activated carbon was also observed to be endothermic [42].

Table 3. Thermodynamic parameters for the adsorption of Pb(II) by biochar.

T (K)	ΔG^0 (kJ/mol)	ΔH^0 (kJ/mol)	ΔS^0 (J/mol·K)
298	−3.060		
308	−2.729	−9.152	−20.576
318	−2.654		

3.7. Optimization of Biochar Adsorption Process

RSM can elucidate the influence of multiple factors and express the interaction between each factor. The Pb(II) removal efficiency under different conditions can be calculated by using response surface equations. Based on the single-factor experimental results of the adsorption of the heavy metal Pb(II) on biochar, the initial concentration of Pb(II) was set to 100 mg/L, and the optimal experimental design were three factors and three levels to accurately obtain the optimal conditions for Pb(II) adsorption on biochar. The design variables were listed in Table 4. The pH values (*A*) of Pb(II)-contaminated wastewater were 4, 5, and 6, the adsorption contact times (*B*) of biochar were 120, 240, and 360 min, and the dose of biochar (*C*) in wastewater were 2, 3, and 4 g/L.

Table 4. Range of variables values for response surface.

Factor	Variables	Unit	Minimum	Maximum	Mean
A	pH value		4	6	5
B	Contact time	min	120	360	240
C	Biochar dose	g/L	2	4	3

The Box–Behnken design (BBD) was used to find the optimal adsorption process conditions [43]. The RSM design results of 17 experimental groups were shown in Table 5. In the response surface experiments, the maximum Pb(II) removal efficiency was 91.62%, the minimum was 87.06%, and the average was 89.05%. According to the range analysis, the order of influence of various factors on the Pb(II) removal was $C > B > A$, that is, the dose of biochar had the largest influence on the adsorption capacity, followed by the adsorption contact time, and pH had the least influence.

The second-order polynomial equations of coded values and actual experimental values were established by multiple regression analysis of the experimental data, as shown in Equations (10) and (11).

$$Y_{\text{Coded}} = 91.47 + 0.3038A + 0.4125B + 0.3112C - 0.3800AB - 0.2825AC + 0.3350BC - 1.49A^2 - 1.68B^2 - 1.98C^2, \quad (10)$$

$$Y_{\text{Actual}} = 20.36050 + 16.81875A + 0.066838B + 12.93852C - 0.003167AB - 0.282500AC + 0.002792BC - 1.49075A^2 - 0.000117B^2 - 1.98075C^2. \quad (11)$$

Table 5. BBD for three independent variables.

Run	pH Value		Contact Time (min)		Biochar Dose (g/L)		Removal Efficiency (%)
	A Actual	Coded	*B* Actual	Coded	*C* Actual	Coded	
1	4	−1	240	0	4	+1	88.56
2	6	+1	360	+1	3	0	88.69
3	6	+1	240	0	4	+1	88.38
4	4	−1	120	−1	3	0	87.16
5	5	0	240	0	3	0	91.22
6	4	−1	360	+1	3	0	88.62
7	5	0	360	+1	2	−1	87.80
8	5	0	120	−1	2	−1	87.52
9	4	−1	240	0	2	−1	87.06
10	5	0	240	0	3	0	91.50
11	6	+1	120	−1	3	0	88.75
12	5	0	240	0	3	0	91.56
13	5	0	120	−1	4	+1	87.16
14	5	0	360	+1	4	+1	88.78
15	5	0	240	0	3	0	91.62
16	6	+1	240	0	2	−1	88.01
17	5	0	240	0	3	0	91.47

Table 6 listed the results of the variance analysis of the BBD model. The lack of fit was 0.3256 and greater than 0.05, indicating that the model was appropriate, because the lack of fit was not significant, and the possibility of distortion was small [44]. The *p*-value is an indicator to measure the difference between the control group and the experimental group. In response surface analysis, the *p*-value was used to determine whether the influence of factors was significant. The $p < 0.05$ indicated that the corresponding factor had significant effect. The variables of pH (*A*), contact time (*B*), and biochar dose (*C*) had significant effects on the adsorption of Pb(II) on biochar in linear terms of (*p*-value < 0.05). In the quadratic model terms, the interaction between pH and contact time (*AB*) as well as between contact time and biochar dose (*BC*) had a significant impact on Pb(II) removal. According to the optimized experiment, the Pb(II) removal efficiency was the highest at a pH of 5, a contact time of 255 min, and a biochar dose of 3 g/L, and the predicted value was 91.52%.

Table 6. ANOVA for Pb(II) adsorption of biochar.

Source	Sum of Squares	df	Mean Square	*F*-Value	*p*-Value
Mode	46.31	9	5.15	85.86	<0.0001
A	0.7381	1	0.7381	12.32	0.0099
B	1.36	1	1.36	22.71	0.0020
C	0.7750	1	0.7750	12.93	0.0088
AB	0.5776	1	0.5776	9.64	0.0172
AC	0.3192	1	0.3192	5.33	0.0543
BC	0.4489	1	0.4489	7.49	0.0290
A^2	9.36	1	9.36	156.14	<0.0001
B^2	11.86	1	11.86	197.89	<0.0001
C^2	16.52	1	16.52	275.66	<0.0001
Residual	0.4195	7	0.0599		
Lack of Fit	0.3256	3	0.1085	4.62	0.0866
Pure Error	0.0939	4	0.0235		
Cor Total	46.73	16			

The R^2 of the fitted model was 0.9910, which met the requirements of the test range. The adjusted R^2 was 0.9795 (Table 7), and the value was close to 1, indicating that the model can explain 97.95% of the response value variation [45]. The regression equation had a high

degree of fit, and the predicted values fitted well with the measured value within the range of the test. The coefficient of variation (*CV*) reflected the variation of the treatment groups at all levels [46], and its value of 0.2749 indicated good reproducibility of the model.

Table 7. Regression equation analysis of response surface.

Std. Dev.	*R*-Squared	Mean	Adj *R*-Squared	C.V. %	Pred *R*-Squared	Adeq Precision
0.2448	0.9910	89.05	0.9795	0.2749	0.8854	23.2698

The three-dimensional response surface and contour plot of the interaction of various factors were shown in Figure 9. The response surface can be plotted by keeping one factor unchanged and changing the other two variables in different experimental ranges. The interaction between pH and contact time (Figure 9a) as well as between contact time and biochar dose (Figure 9c) was significant. The analysis of variance (Table 6) also confirmed this result, with *p*-values of 0.0172 and 0.0290, respectively. The three-dimensional response surface and contour map of Pb(II) removal with pH and contact time under the condition of constant biochar dose (3 g/L) were shown in Figure 9a. With the increase in pH and contact time, the Pb(II) removal efficiency increased rapidly and then decreased. This trend might be explained by the presence of a limited number of adsorption sites on the surface of biochar, and high or low pH value will reduce the quantity of ligand exchange between Pb(II) ions and biochar, affecting its adsorption performance. The Pb(II) removal efficiency per unit mass of biochar decreased with the increase in biochar dose (Figure 9c), which was related to the equilibrium of Pb(II) adsorption and desorption. However, as indicated in Figure 9b, the interaction between pH and biochar dose was not very significant, which was consistent with the ANOVA results (p = 0.0543 > 0.05). The experimental result of the Pb(II) removal efficiency of 89.02% was obtained at the optimal adsorption conditions, which was consistent with the predicted value (91.52%) established from the model.

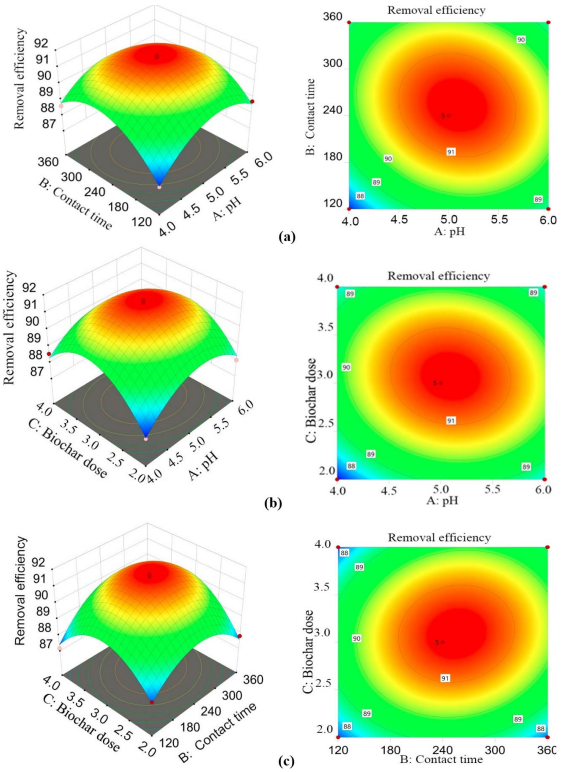

Figure 9. Contour plot and 3-D surface plot of Pb(II) adsorption. (**a**) interaction between pH and contact time; (**b**) interaction between pH and biochar dose; (**c**) interaction between contact time and biochar dose.

3.8. Assessment of the Pb(II) Removal Performance

In order to compare the adsorption capacity of the biochar with various adsorbents from agricultural waste, Table 8 provided a summary of the experimental data that have been published related to the adsorption of Pb(II). Although the corn straw biochar showed lower Pb(II) adsorption capacities, it had a better effect than that of untreated corn straw. In view of the low utilization rate of a large number of corn stalks in the local area and the environmental pollution caused by them, it was an eco-friendly solution to remove Pb(II) from wastewater with cornstraw biochar.

Table 8. Summary of the literature related to Pb(II) adsorption capacities of some adsorbents from agricultural waste.

Adsorbent	q_{max} (mg/g)	References
Peanut Shell	7.1	[47]
Corn straw	15.03	[12]
Castor oil cake biochar	15.9	[48]
Corn straw biochar	21.6	This study
Peanut hull biochar	22.8	[18]
Rice husk biochar	36.73	[49]
Esterified corncobs	43.4	[50]
Coconut shell biochar	47.2	[51]
Corn stalk biochar	49.7	[21]
Peanut shells biochar	56.5	[19]
Coconut shell-based biochar by ultraviolet (UV) irradiation	66.86	[52]
Cotton straw-derived biochar	124.7	[20]
Kiwi branch biochar modified with Zn-Fe (KB/Zn-Fe)	161.29	[53]
Corn stalk biochar	352	[54]
Ragweed biochar	358.7	[55]
Red mud modified rice-straw biochar	426.84	[22]

4. Conclusions

Biochar has been identified as a promising material for treating Pb-contaminated wastewater. The Pb(II) adsorption process of biochar could be classified as mainly heterogeneous adsorption with multi-molecular layers, and a weakly acidic environment was more conducive to ligand exchange between Pb(II) ions and biochar. With the increase in biochar dose, the removal efficiency of Pb(II) increased, and the removal efficiency reached 90.31% at a Pb(II) concentration of 100 mg/L. In addition, Pseudo-first-order model was more suitable to describe the adsorption process on biochar. The adsorption amount of Pb(II) at 240 min was 20.8 mg/g, which was 93.37% of the saturated adsorption capacity. Simultaneously, the result of response surface analysis demonstrated that the maximum predicted removal efficiency of Pb(II) reached 91.52% at a pH of 5, an adsorption contact time of 255 min, and a biochar dose of 3 g/L.

Author Contributions: Conceptualization, Y.J. and W.Y.; Resources, B.L.; investigation, C.Y., G.L., B.W. and X.Z.; data curation, B.L., C.Y., G.L., B.W. and X.Z.; formal analysis, C.L., Y.J. and W.Y.; validation, J.Z. and S.Q.; visualization, Y.J.; writing—original draft preparation, Y.J. and C.L.; writing—review and editing, W.Y., B.L., J.Z. and S.Q.; funding acquisition, W.Y. and G.L. All authors have read and agreed to the published version of the manuscript.

Funding: This research was funded by the National Natural Science Foundation of China grant number 31800361, Henan Provincial Science and Technology Research Project grant number 222102110101, and Project of Henan Academy of Sciences, grant number 220605055.

Data Availability Statement: Not applicable.

Conflicts of Interest: The authors declare no conflict of interest.

References

1. Oliveira, M.L.S.; Izquierdo, M.; Querol, X.; Lieberman, R.N.; Saikia, B.K.; Silva, L.F.O. Nanoparticles from construction wastes: A problem to health and the environment. *J. Clean. Prod.* **2019**, *219*, 236–243. [CrossRef]
2. Tang, Q.; Wang, K.; Yaseen, M.; Tong, Z.; Cui, X. Synthesis of highly efficient porous inorganic polymer microspheres for the adsorptive removal of Pb^{2+} from wastewater. *J. Clean. Prod.* **2018**, *193*, 351–362. [CrossRef]
3. Hazrati, S.; Farahbakhsh, M.; Heydarpoor, G.; Besalatpour, A.A. Mitigation in availability and toxicity of multi-metal contaminated soil by combining soil washing and organic amendments stabilization. *Ecotox. Environ. Safe.* **2020**, *201*, 110807. [CrossRef] [PubMed]
4. Chen, L.; Zhou, S.; Wu, S.; Wang, C.; He, D. Concentration, fluxes, risks, and sources of heavy metals in atmospheric deposition in the Lihe River watershed, Taihu region, eastern China. *Environ. Pollut.* **2019**, *255*, 113301. [PubMed]
5. Chen, Y.; Zhang, X.; Chen, W.; Yang, H.; Chen, H. The structure evolution of biochar from biomass pyrolysis and its correlation with gas pollutant adsorption performance. *Bioresour. Technol.* **2017**, *246*, 101–109. [CrossRef] [PubMed]
6. Gu, X.C.; Mei, P.Y.; Zhang, Z.; Jiang, W.; Li, X.R. Research progress on treatment technology of lead-bearing wastewater. *Ind. Water. Treat.* **2020**, *40*, 14–19.
7. Liu, G.; Liao, L.; Dai, Z.; Qi, Q.; Wu, J.; Ma, L.Q.; Tang, C.; Xu, J. Organic adsorbents modified with citric acid and Fe_3O_4 enhance the removal of Cd and Pb in contaminated solutions. *Chem. Eng. J.* **2020**, *395*, 125108. [CrossRef]
8. Jin, Y.; Teng, C.; Yu, S.; Song, T.; Dong, L.; Liang, J.; Bai, X.; Liu, X.; Hu, X.; Qu, J. Batch and fixed-bed biosorption of Cd(II) from aqueous solution using immobilized *Pleurotus ostreatus* spent substrate. *Chemosphere* **2018**, *191*, 799–808. [CrossRef] [PubMed]
9. Liu, X.; Bai, X.; Dong, L.; Liang, J.; Jin, Y.; Wei, Y.; Li, Y.; Huang, S.; Qu, J. Composting enhances the removal of lead ions in aqueous solution by spent mushroom substrate: Biosorption and precipitation. *J. Clean. Prod.* **2018**, *200*, 1–11.
10. Lyu, H.D. Study on Adsorption Characteristics of Heavy Metals from Wastewater Treatment Residuals. Master's Thesis, Beijing University of Civil Engineering and Architecture, Beijing, China, 2020.
11. Yang, D.; Li, T.; Nie, Y.; Ren, J.; Rao, N.; Ma, X. Research progress of biomass adsorption materials in water pollution treatment. *Shandong Chem. Ind.* **2022**, *51*, 187–188+192.
12. Jia, D.; Li, C. Adsorption of Pb(II) from aqueous solutions using corn straw. *Desalination Water Treat.* **2015**, *56*, 223–231. [CrossRef]
13. Regkouzas, P.; Diamadopoulos, E. Adsorption of selected organic micro-pollutants on sewage sludge biochar. *Chemosphere* **2019**, *224*, 840–851. [CrossRef] [PubMed]
14. Ma, Y.; Liu, W.-J.; Zhang, N.; Li, Y.-S.; Jiang, H.; Sheng, G.-P. Polyethylenimine modified biochar adsorbent for hexavalent chromium removal from the aqueous solution. *Bioresour. Technol.* **2014**, *169*, 403–408. [CrossRef] [PubMed]
15. Lu, C.; Li, W.; Zhang, Q.; Liu, L.; Zhang, N.; Qu, B.; Yang, X.; Xu, R.; Chen, J.; Sun, Y. Enhancing photo-fermentation biohydrogen production by strengthening the beneficial metabolic products with catalysts. *J. Clean. Prod.* **2021**, *317*, 128437. [CrossRef]
16. Li, J.; Liang, M.; Wang, D.; Lu, L.; Zhu, Y. Advances in the study of lead adsorption by biochar and its composites. *Environ. Sci. Technol.* **2021**, *44*, 163–171.
17. Mu, R.M.; Wang, M.X.; Bu, Q.W.; Liu, D.; Zhao, Y.L. Adsorption of Pb(II) from aqueous solutions by wheat straw biochar. *IOP Conf. Ser. Earth Environ. Sci.* **2018**, *191*, 012041. [CrossRef]
18. Xue, Y.; Gao, B.; Yao, Y.; Inyang, M.; Zhang, M.; Zimmerman, A.R.; Ro, K.S. Hydrogen peroxide modification enhances the ability of biochar (hydrochar) produced from hydrothermal carbonization of peanut hull to remove aqueous heavy metals: Batch and column tests. *Chem. Eng. J.* **2012**, *200–202*, 673–680.
19. Taşar, Ş.; Özer, A. A Thermodynamic and Kinetic Evaluation of the adsorption of Pb(II) ions using peanut (*Arachis Hypogaea*) shell-based biochar from aqueous media. *Pol. J. Environ. Stud.* **2019**, *29*, 293–305. [CrossRef]
20. Wang, Z.; Xu, J.; Yellezuome, D.; Liu, R. Effects of cotton straw-derived biochar under different pyrolysis conditions on Pb (II) adsorption properties in aqueous solutions. *J. Anal. Appl. Pyrolysis* **2021**, *157*, 105214. [CrossRef]
21. Liu, L.; Huang, Y.; Zhang, S.; Gong, Y.; Su, Y.; Cao, J.; Hu, H. Adsorption characteristics and mechanism of Pb(II) by agricultural waste-derived biochars produced from a pilot-scale pyrolysis system. *Waste Manage.* **2019**, *100*, 287–295. [CrossRef]
22. Waqas, A.; Sajid, M.; Mohsin, M.; Sehrish, A.; Awais, S.; Avelino, N.; Ammar, A.R.M.; Hongwei, Z.; Wenjie, L.; Weidong, L. Adsorption of Pb(II) from wastewater using a red mud modified rice-straw biochar: Influencing factors and reusability. *Environ. Pollut.* **2023**, *326*, 121405.
23. Lian, Q.; Ahmad, Z.U.; Gang, D.D.; Zappi, M.E.; Fortela, D.L.B.; Hernandez, R. The effects of carbon disulfide driven functionalization on graphene oxide for enhanced Pb(II) adsorption: Investigation of adsorption mechanism. *Chemosphere* **2020**, *248*, 126078. [PubMed]
24. Wei, D.; Huo, W.; Li, G.; Xie, Q.; Jiang, Y. The combined effects of lysozyme and ascorbic acid on microstructure and properties of zein-based films. *Chin. J. Chem. Eng.* **2018**, *26*, 648–656. [CrossRef]
25. Hoppen, M.I.; Carvalho, K.Q.; Ferreira, R.C.; Passig, F.H.; Pereira, I.C.; Rizzo-Domingues, R.C.P.; Lenzi, M.K.; Bottini, R.C.R. Adsorption and desorption of acetylsalicylic acid onto activated carbon of babassu coconut mesocarp. *J. Environ. Chem. Eng.* **2018**, *7*, 102862. [CrossRef]
26. Babić, B.M.; Milonjić, S.K.; Polovina, M.J.; Kaludierović, B.V. Point of zero charge and intrinsic equilibrium constants of activated carbon cloth. *Carbon* **1999**, *37*, 477–481. [CrossRef]

27. Al-Jubouri, S.M.; Curry, N.A.; Holmes, S.M. Hierarchical porous structured zeolite composite for removal of ionic contaminants from waste streams and effective encapsulation of hazardous waste. *J. Hazard. Mater.* **2016**, *320*, 241–251. [CrossRef] [PubMed]
28. Wang, J.; Ji, Y.; Ding, S.; Ma, H.; Han, X. Adsorption and desorption behavior of tannic acid in aqueous solution on polyaniline adsorbent. *Chin. J. Chem. Eng.* **2013**, *21*, 594–599. [CrossRef]
29. Ma, K.Y.; Zhang, H.; Song, N.N.; Wang, F.L.; Lin, D.S. Mechanism of cadmium adsorption by oxidative aging corn straw biochar. *J. Agro-Environ. Sci.* **2022**, *41*, 1230–1240.
30. Zhang, G.S.; Cheng, H.Y.; Zhang, H.B.; Su, L.; He, X.F.; Tian, X.; Ning, R.Y. Adsorption mechanism of Pb^{2+} in water by biochar derived from spent Agaricus bisporus substrate and its environmental application potential. *J. Agro-Environ. Sci.* **2021**, *40*, 659–667.
31. Zhang, J.S.; Stanforth, R. Slow adsorption reaction between arsenic species and goethite (alpha-FeOOH): Diffusion or heterogeneous surface reaction control. *Langmuir* **2005**, *21*, 2895–2901. [CrossRef]
32. Zhang, X.; Gang, D.D.; Sun, P.; Lian, Q.; Yao, H. Goethite dispersed corn straw-derived biochar for phosphate recovery from synthetic urine and its potential as a slow-release fertilizer. *Chemosphere* **2021**, *262*, 127861. [CrossRef]
33. Mohan, D.; Pittman, C.U., Jr.; Bricka, M.; Smith, F.; Yancey, B.; Mohammad, J.; Steele, P.H.; Alexandre-Franco, M.F.; Gómez-Serrano, V.; Gong, H. Sorption of arsenic, cadmium, and lead by chars produced from fast pyrolysis of wood and bark during bio-oil production. *J. Colloid Interface Sci.* **2007**, *310*, 57–73. [CrossRef] [PubMed]
34. Shen, Z.; Tian, D.; Zhang, X.; Tang, L.; Su, M.; Zhang, L.; Li, Z.; Hu, S.; Hou, D. Mechanisms of biochar assisted immobilization of Pb^{2+} by bioapatite in aqueous solution. *Chemosphere* **2018**, *190*, 260–266. [CrossRef] [PubMed]
35. Jiang, J.; Long, Y.; Hu, X.; Hu, J.; Zhu, M.; Zhou, S. A facile microwave-assisted synthesis of mesoporous hydroxyapatite as an efficient adsorbent for Pb^{2+} adsorption. *J. Solid State Chem.* **2020**, *289*, 121491. [CrossRef]
36. Lin, P.-Y.; Wu, H.-M.; Hsieh, S.-L.; Li, J.-S.; Dong, C.; Chen, C.-W.; Hsieh, S. Preparation of vaterite calcium carbonate granules from discarded oyster shells as an adsorbent for heavy metal ions removal. *Chemosphere* **2020**, *254*, 126903. [CrossRef]
37. Dong, S.X.; Wang, Y.L.; Zhao, Y.W.; Zhou, X.H.; Zheng, H.L. $La^{3+}/La(OH)_{(3)}$ loaded magnetic cationic hydrogel composites for phosphate removal: Effect of lanthanum species and mechanistic study. *Water Res.* **2017**, *126*, 433–441. [CrossRef]
38. Deng, H.; Lu, J.; Li, G.; Zhang, G.; Wang, X. Adsorption of methylene blue on adsorbent materials produced from cotton stalk. *Chem. Eng. J.* **2011**, *172*, 326–334. [CrossRef]
39. Zhang, Y.; Wang, Y.; Zhang, H.; Li, Y.; Zhang, Z.; Zhang, W. Recycling spent lithium-ion battery as adsorbents to remove aqueous heavy metals: Adsorption kinetics, isotherms, and regeneration assessment. *Resour. Conserv. Recycl.* **2020**, *156*, 104688. [CrossRef]
40. Zhang, Z.; Wang, T.; Zhang, H.; Liu, Y.; Xing, B. Adsorption of Pb(II) and Cd(II) by magnetic activated carbon and its mechanism. *Sci. Total. Environ.* **2021**, *757*, 143910. [CrossRef] [PubMed]
41. Al-Ghouti, M.A.; Da'ana, D.A. Guidelines for the use and interpretation of adsorption isotherm models: A review. *J. Hazard. Mater.* **2020**, *393*, 122383. [CrossRef] [PubMed]
42. Medhat, A.; El-Maghrabi, H.H.; Abdelghany, A.; Menem, N.M.A.; Raynaud, P.; Moustafa, Y.M.; Elsayed, M.A.; Nada, A.A. Efficiently activated carbons from corn cob for methylene blue adsorption. *Appl. Surf. Sci. Adv.* **2021**, *3*, 100037. [CrossRef]
43. Li, Y.; Zhang, Z.; Jing, Y.; Ge, X.; Wang, Y.; Lu, C.; Zhou, X.; Zhang, Q. Statistical optimization of simultaneous saccharification fermentative hydrogen production from *Platanus orientalis* leaves by photosynthetic bacteria HAU-M1. *Int. J. Hydrog. Energy* **2017**, *42*, 5804–5811. [CrossRef]
44. Lu, C.; Jing, Y.; Zhang, H.; Lee, D.-J.; Tahir, N.; Zhang, Q.; Li, W.; Wang, Y.; Liang, X.; Wang, J.; et al. Biohydrogen production through active saccharification and photo-fermentation from alfalfa. *Bioresour. Technol.* **2020**, *304*, 123007. [CrossRef] [PubMed]
45. Jing, Y.; Li, F.; Li, Y.; Jin, P.; Zhu, S.; He, C.; Zhao, J.; Zhang, Z.; Zhang, Q. Statistical optimization of simultaneous saccharification fermentative hydrogen production from corn stover. *Bioengineered* **2019**, *11*, 428–438. [CrossRef]
46. Lu, C.; Zhang, Z.; Ge, X.; Wang, Y.; Zhou, X.; You, X.; Liu, H.; Zhang, Q. Bio-hydrogen production from apple waste by photosynthetic bacteria HAU-M1. *Int. J. Hydrogen Energy* **2016**, *41*, 13399–13407. [CrossRef]
47. OuYang, X.-K.; Yang, L.-P.; Wen, Z.-S. Adsorption of Pb(II) from solution using peanut shell as biosorbent in the presence of amino acid and sodium chloride. *BioResources* **2014**, *9*, 2446–2458. [CrossRef]
48. Kalinke, C.; Mangrich, A.S.; Marcolino-Junior, L.H.; Bergamini, M.F. Biochar prepared from castor oil cake at different temperatures: A voltammetric study applied for Pb^{2+}, Cd^{2+} and Cu^{2+} ions preconcentration. *J. Hazard. Mater.* **2016**, *318*, 526–532. [CrossRef]
49. Li, Y.; Liu, X.; Zhang, P.; Wang, X.; Cao, Y.; Han, L. Qualitative and quantitative correlation of physicochemical characteristics and lead sorption behaviors of crop residue-derived chars. *Bioresour. Technol.* **2018**, *270*, 545–553. [CrossRef]
50. Tan, G.; Yuan, H.; Liu, Y.; Xiao, D. Removal of lead from aqueous solution with native and chemically modified corncobs. *J. Hazard. Mater.* **2009**, *174*, 740–745. [CrossRef]
51. Largitte, L.; Gervelas, S.; Tant, T.; Dumesnil, P.C.; Hightower, A.; Yasami, R.; Bercion, Y.; Lodewyckx, P. Removal of lead from aqueous solutions by adsorption with surface precipitation. *Adsorption* **2014**, *20*, 689–700. [CrossRef]
52. Qiao, L.; Yutao, G.; Jian, L.; Wenchuan, D.; Yi, Y. Removal of Pb(II) and Cu(II) from aqueous solutions by ultraviolet irradiation-modified biochar. *Desalin. Water Treat.* **2017**, *82*, 179–187.
53. Tan, Y.; Wan, X.; Zhou, T.; Wang, L.; Yin, X.; Ma, A.; Wang, N. Novel Zn-Fe engineered kiwi branch biochar for the removal of Pb(II) from aqueous solution. *J. Hazard. Mater.* **2022**, *424*, 127349. [CrossRef] [PubMed]

54. Wang, S.; Guo, W.; Gao, F.; Yang, R. Characterization and Pb(II) removal potential of corn straw- and municipal sludge-derived biochars. *R. Soc. Open Sci.* **2017**, *4*, 170402. [CrossRef] [PubMed]
55. Lian, W.; Yang, L.; Joseph, S.; Shi, W.; Bian, R.; Zheng, J.; Li, L.; Shan, S.; Pan, G. Utilization of biochar produced from invasive plant species to efficiently adsorb Cd (II) and Pb (II). *Bioresour. Technol.* **2020**, *317*, 124011. [CrossRef]